Quantifying the Coverage Density of Poly(ethylene glycol) Chains on the Surface of Gold Nanostructures

Xiaohu Xia,[†,§,¶] Miaoxin Yang,[†,¶] Yucai Wang,[†] Yiqun Zheng,[⊥] Qingge Li,[§] Jingyi Chen,[*,†,‡] and Younan Xia[*,†,#]

[†]Department of Biomedical Engineering, Washington University, St. Louis, Missouri 63130, United States, [‡]Department of Chemistry and Biochemistry, University of Arkansas, Fayetteville, Arkansas 72701, United States, [§]Engineering Research Center of Molecular Diagnostics, School of Life Sciences, Xiamen University, Xiamen, Fujian 361005, P. R. China, and [⊥]Department of Chemistry, Washington University, St. Louis, Missouri 63130, United States. [¶]These two authors contributed equally to this work. [#]Present address: The Wallace H. Coulter Department of Biomedical Engineering, Georgia Institute of Technology and Emory University Medical School, and School of Chemistry and Biochemistry, Georgia Institute of Technology, Atlanta, Georgia 30332, United States.

ABSTRACT

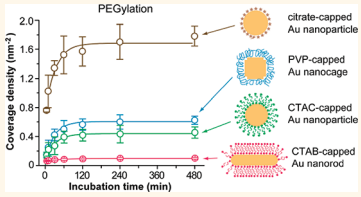

The coverage density of poly(ethylene glycol) (PEG) is a key parameter in determining the efficiency of PEGylation, a process pivotal to *in vivo* delivery and targeting of nanomaterials. Here we report four complementary methods for quantifying the coverage density of PEG chains on various types of Au nanostructures by using a model system based on HS—PEG—NH_2 with different molecular weights. Specifically, the methods involve reactions with fluorescamine and ninhydrin, as well as labeling with fluorescein isothiocyanate (FITC) and Cu^{2+} ions. The first two methods use conventional amine assays to measure the number of unreacted HS—PEG—NH_2 molecules left behind in the solution after incubation with the Au nanostructures. The other two methods involve coupling between the terminal —NH_2 groups of adsorbed —S—PEG—NH_2 chains and FITC or a ligand for Cu^{2+} ion, and thus pertain to the "active" —NH_2 groups on the surface of a Au nanostructure. We found that the coverage density decreased as the length of PEG chains increased. A stronger binding affinity of the initial capping ligand to the Au surface tended to reduce the PEGylation efficiency by slowing down the ligand exchange process. For the Au nanostructures and capping ligands we have tested, the PEGylation efficiency decreased in the order of citrate-capped nanoparticles > PVP-capped nanocages ≈ CTAC-capped nanoparticles ≫ CTAB-capped nanorods, where PVP, CTAC, and CTAB stand for poly(vinyl pyrrolidone), cetyltrimethylammonium chloride, and cetyltrimethylammonium bromide, respectively.

KEYWORDS: Au nanostructure · PEGylation · ligand exchange · capping ligand

Inorganic nanomaterials have attracted widespread interest as a multifunctional platform for various applications in biology and medicine.[1−3] Among them, Au nanostructures have been used as both imaging and therapeutic agents for diagnosis and treatment of diseases such as cancer.[4−10] To be useful *in vivo*, it is critical to have the nanoparticles delivered to the site of interest without being accumulated in healthy tissues and organs. The nanoparticles, therefore, must have the ability to bypass the reticuloendothelial system (RES), circulate in the bloodstream for a long period of time, and preferentially accumulate at the site of interest. Poly(ethylene glycol) (PEG) is the most widely used polymer for masking nanoparticles from clearance by RES due to its ability to resist protein adsorption, excellent biocompatibility, and commercial availability.[11−14] The success of PEGylation critically depends on the coverage density of PEG chains on the surface of a nanoparticle, herein referred to as the number of PEG chains per nm^2 of the particle surface. Essentially, the coverage density of PEG chains represents one of the key parameters in determining the efficiency of PEGylation and thereby the protein repelling capability of resultant nanoparticles and their circulation half-life.[15,16]

PEGylation of Au nanostructures is typically achieved through a ligand exchange process by using thiol-terminated PEG molecules.[17−19] For chemically synthesized Au nanostructures, they are often covered and stabilized by different capping ligands depending on the protocols. During PEGylation, the capping ligands are displaced by —S—PEG chains due to a stronger Au—S linkage and an energy gain associated with the intermolecular interaction.[20] Different methods have been employed to assess the efficiency of PEGylation, including those that directly measure changes to the physical properties of nanoparticles such as solubility, stability, hydrodynamic diameter, and zeta potential. None of these methods, however, can provide quantitative information with regard to the number of PEG

* Address correspondence to younan.xia@bme.gatech.edu, chenj@uark.edu.

Received for review October 6, 2011 and accepted December 11, 2011.

Published online December 11, 2011
10.1021/nn2038516

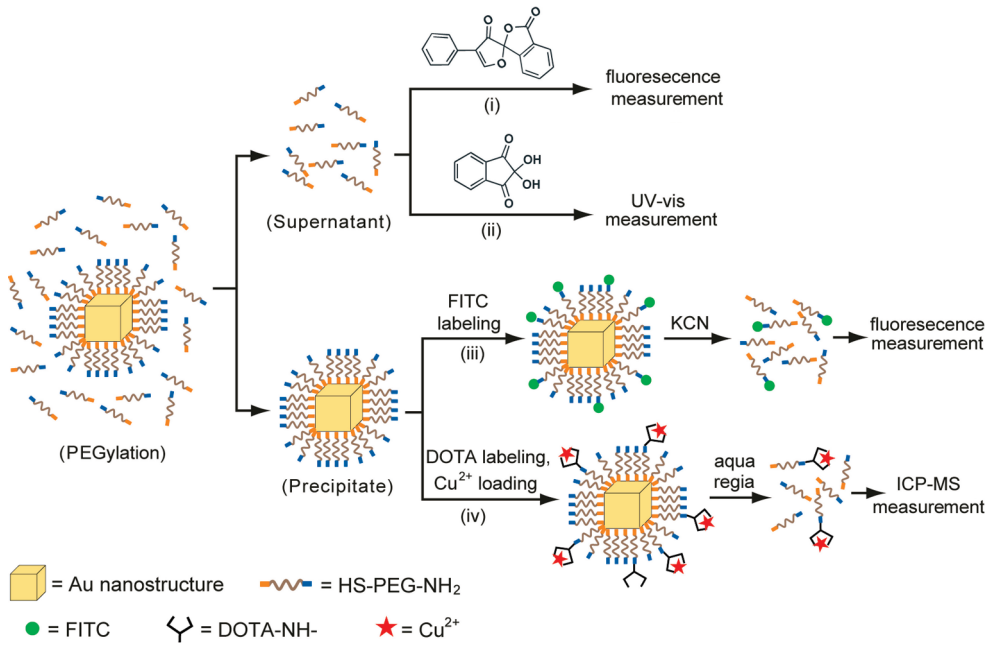

Figure 1. Schematic illustration of the four methods for quantifying the average number of $-S-PEG-NH_2$ chains on the surface of one single Au nanostructure: (i) fluorescamine-based assay, (ii) ninhydrin-based assay, (iii) FITC-labeling assay, and (iv) Cu^{2+}-labeling assay.

chains on the surface of a particle. Thermal gravity analysis (TGA) has been widely used to estimate the number of PEG chains on the surface of a nanoparticle.[21] It measures the mass difference before and after removal of PEG chains due to thermal desorption and decomposition. To measure the mass change accurately, it requires the use of a relatively large quantity of the sample. The coverage density calculated from TGA data corresponds to the total number of PEG chains in the sample, including those loosely trapped among the particles. When the other end of a PEG chain is terminated in a different functional group like $-NH_2$, not all the terminal groups can be activated and coupled to another ligand such as a targeting moiety. In this case, there is also a critical need to quantify both the total and "active" $-PEG-NH_2$ chains on the surface of a Au nanoparticle. Here we accomplish this goal by using a combination of four complementary methods.

We focused on $HS-PEG-NH_2$ molecules with different molecular weights because $-NH_2$ is one of the most commonly used functional group for further conjugation through amide coupling with the carboxylate or carboxylic acid group.[22,23] Various reagents such as fluorescamine and ninhydrin have been used to quantitatively analyze the number of primary amines in small molecules, peptides, and proteins.[24−26] The fluorescamine-based assay involves the production of a fluorescent compound that can be quantified by fluorescence spectroscopy with high sensitivity while the ninhydrin-based assay yields a chromophore with strong absorption in the visible that can be measured using ultraviolet−visible (UV−vis) spectroscopy. In this article, we apply these two assays to quantify the total number of $HS-PEG-NH_2$ molecules left behind in the reaction solution after incubation with various types of Au nanostructures. We determined the coverage density of $-S-PEG-NH_2$ chains on the surface of a Au nanostructure and systematically studied the adsorption kinetics of $HS-PEG-NH_2$ with different molecular weights. We also compared the PEGylation efficiencies for Au nanostructures with different morphologies and/or initially capped by different types of ligands. At the same time, we developed two new methods for quantitatively measuring the number of "active" $-S-PEG-NH_2$ chains on the surface of a Au nanostructure using assays based on dye- and Cu^{2+}-labeling. This study provides a set of useful guidelines for the PEGylation of Au nanostructures toward a range of biomedical applications.

RESULTS AND DISCUSSION

We used four different methods to measure the coverage density of $-S-PEG-NH_2$ chains on the surface of a Au nanostructure, including fluorescence assays based on fluorescamine and fluorescein isothiocyanate (FITC)-labeling, UV−vis spectroscopy assay involving ninhydin, and inductively coupled plasma mass spectrometry (ICP−MS) analysis based on Cu^{2+}-labeling. Figure 1 schematically illustrates the principles of these four methods. Both the fluorescamine- and ninhydrin-based assays measure the concentration of unreacted $HS-PEG-NH_2$ molecules left behind in the supernatant of a sample using fluorescence and UV−vis absorption, respectively. These two methods yield the total number of $-S-PEG-NH_2$ chains on the entire surface of all Au

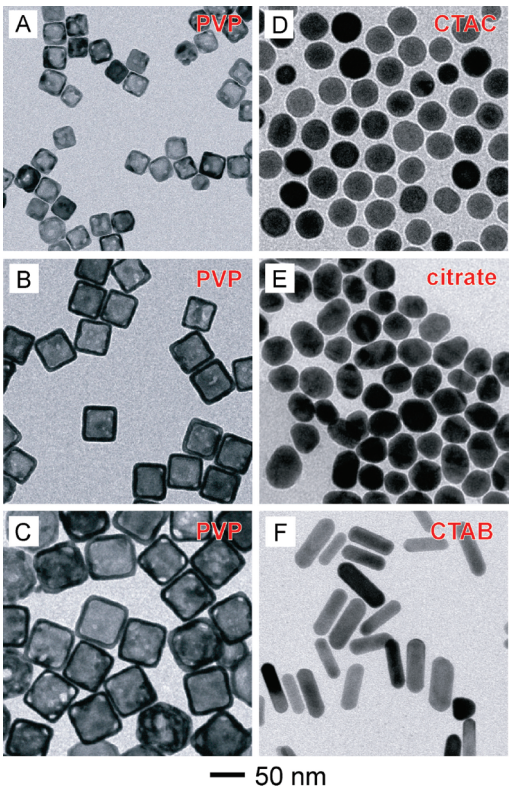

Figure 2. TEM images of the different types of Au nanostructures used in this work: (A, B, C) PVP-capped AuNCs with average edge lengths of 30, 50, and 60 nm, respectively; (D) CTAC-capped AuNPs with an avarage diameter of 40 nm; (E) citrate-capped AuNPs with an avarage diameter of 42 nm; and (F) CTAB-capped AuNRs with avarage dimensions of 80 nm × 22 nm.

nanostructures in the sample after the amount of HS−PEG−NH_2 remaining in the supernatant has been subtracted from the amount of HS−PEG−NH_2 added to the original solution. For the other two methods, the Au−S−PEG−NH_2 conjugates are labeled with FITC molecules or Cu^{2+} ions and precipitated out from the solution for fluorescence and ICP−MS measurements, respectively, after the Au nanostructures have been selectively dissolved with an etching solution. The outputs of these two methods are the coverage densities of "active" −S−PEG−NH_2 chains on the surface of a Au nanostructure that could be labeled with FITC or Cu^{2+}.

Synthesis of Au Nanostructures and PEGylation of Their Surfaces *via* Ligand Exchange. Gold nanostructures were prepared with four different capping ligands: poly(vinyl pyrrolidone) (PVP), cetyltrimethylammonium chloride (CTAC), cetyltrimethylammonium bromide (CTAB), and citrate ions. Their surfaces were then modified with HS−PEG−NH_2 using a ligand exchange process. Figure 2 shows TEM images of PVP-capped Au nanocages (AuNCs) with edge lengths of 30, 50, and 60 nm, respectively; CTAC-capped Au nanoparticles (AuNPs) with an avarage diameter of 40 nm; citrate-capped AuNPs with an avarage diameter of 42 nm; and

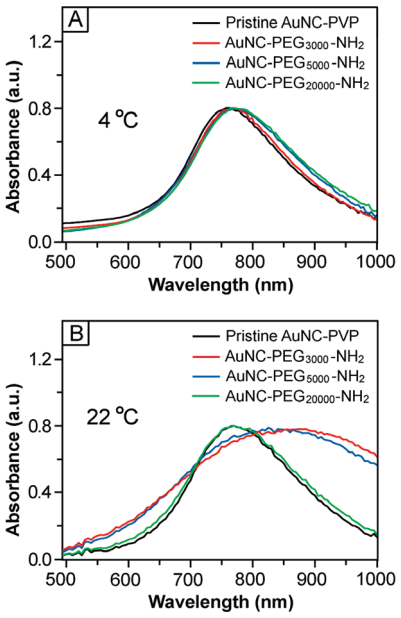

Figure 3. UV−vis spectra of 50-nm AuNCs before and after functionalization with HS−PEG−NH_2 at two different temperatures: (A) 4 and (B) 22 °C. Note that the AuNCs showed significant broadening for their peaks due to aggregation when they were functionalized with HS-PEG_{3000}−NH_2 or HS−PEG_{5000}−NH_2 at 22 °C.

CTAB-capped Au nanorods (AuNRs) with avarage dimensions of 80 nm × 22 nm.

During ligand exchange, HS−PEG−NH_2 could displace the original capping ligand on the surface of a Au nanostructure thanks to a relatively strong Au−S bond and the energy gained through intermolecular interactions between the PEG chains. Interestingly, the outcome of a ligand exchange process was found to have a strong dependence on the reaction temperature for PEG chains with relatively low molecular weights (*e.g.*, PEG_{3000} and PEG_{5000}). The localized surface plasmon resonance (LSPR) peak of the AuNCs only showed very minor red-shifts after incubation with HS−PEG−NH_2 in three different molecular weights at 4 °C (Figure 3A), which can be ascribed to the slight changes in reflective index at the interface. The LSPR peak was essentially retained in shape and width, implying that the AuNCs remained to be well dispersed in the medium after ligand exchange and no aggregation had occurred. When conducted at 22 °C, however, the LSPR peak of the AuNCs was significantly broadened after surface modification with PEG chains of 3000 and 5000 in molecular weight (Figure 3B), indicating that aggregation had occurred in the system. When a PEG of 20000 in molecular weight was used, no aggregation was observed. In addition, the PVP-covered AuNCs showed no change to its UV−vis spectrum when the sample was aged at 4 and 22 °C (Supporting Information, Figure S1). We observed no change to the spectrum either when the PVP-covered AuNCs were conjugated with HS−PEG−COOH at 4 °C while the

peak intensity was slightly reduced when the conjugation was conducted at 22 °C. These results were consistent with the particle sizes and zeta potentials measured by dynamic light scattering (DLS) (Supporting Information, Table S1). The aggregation observed for both samples involving HS−PEG_{3000}−NH_2 and HS−PEG_{5000}−NH_2 at 22 °C can be attributed to the direct connection of two AuNCs by HS−PEG−NH_2 and/or to the presence of some thiol groups on the outmost surface of AuNCs, which are susceptible to cross-linking *via* the formation of a disulfide (S−S) bond between two AuNCs. At 22 °C, both the −NH_2 and −SH groups of a HS−PEG−NH_2 molecule could interact with a Au surface to generate Au−S and Au−N bonds with energies in the range of 30−40 kcal/mol[27] and 5−10 kcal/mol,[28,29] respectively. At 4 °C, however, the Au−S bond was preferentially formed over the Au−N bond probably due to a kinetic reason, leading to the presence of fewer −SH groups on the outer surface. Such a dependence of selectivity on temperature was also observed by other groups for thiol molecules terminated in the amino group.[30] As a result, we observed a more positively charged surface and less significant aggregation for the AuNCs conjugated with HS−PEG−NH_2 of the same molecular weight at 4 °C than those at 22 °C. This phenomenon, however, was not observed for PEG of 20000 in molecular weight probably due to its randomly coiled conformation.[31,32]

Quantification Using the Fluorescamine-Based Assay. The fluorescamine-based assay was originally developed for quantification of primary amines in biomolecules with sensitivity on the pM scale.[24] In this assay, nonfluorescent fluorescamine reacts with a primary amine to generate a fluorescent product that emits light at 480 nm when excited at 390 nm (Figures S2 and S3 in the Supporting Information). Figure 4A shows a calibration curve that correlates the fluorescence intensity at 480 nm with the concentration of HS−PEG−NH_2. The assay was performed under a basic condition (pH 10), and the typical fluorescence spectra are shown in Supporting Information, Figure S4A. Similar to primary aliphatic amine, the pK_a of the amine terminus in HS−PEG−NH_2 is in the range of 9−11.[33] At an acidic pH (*e.g.*, 6.5), the protonated amine could not react with fluorescamine effectively, resulting in a poor linearity for the calibration curve (Supporting Information, Figure S5). In a basic solution, the primary amine was deprotonated and thus became highly reactive toward fluorescamine. Linear relationships were found up to μM concentrations with the slopes decreasing in the order of HS−PEG_{3000}−NH_2 > HS−PEG_{5000}−NH_2 > HS−PEG_{20000}−NH_2. This trend suggests that the amine terminus of PEGs with low molecular weights reacted with fluorescamine more efficiently than those with high molecular weights. Previous studies showed that a helical conformation was preferred by PEG due to the formation of hydrogen bonds between the

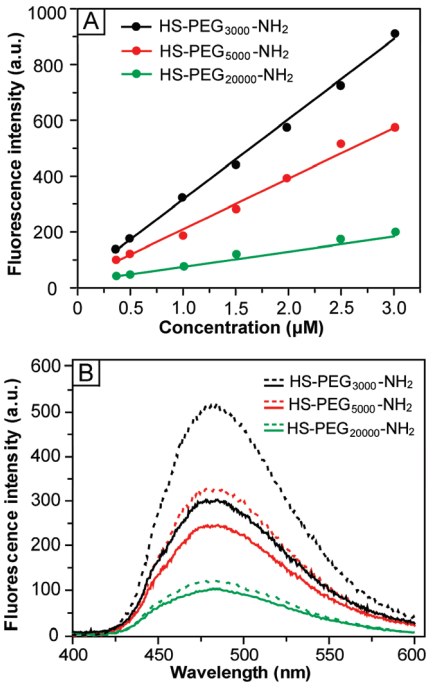

Figure 4. (A) Calibration curves for HS−PEG−NH_2 and fluorescamine-based assay at pH = 10, showing a linear relationship between the fluorescence intensity at 480 nm and the concentration of HS−PEG−NH_2. (B) Fluorescence spectra corresponding to the chromophore derived from a reaction between fluorescamine and HS−PEG_{3000}−NH_2 (black curves), HS−PEG_{5000}−NH_2 (red curves), and HS−PEG_{20000}−NH_2 (green curves), respectively. The dotted and solid curves correspond to the spectra taken from the original solution and the supernatant after incubation with 50-nm AuNCs for 12 h, respectively.

neighboring oxygen atoms and water molecules.[34,35] As such, all the amino groups will be completely exposed at the surface. When the molecular weight of PEG is increased beyond a certain number, however, the helical structure will become less favored. The random coil conformation taken by the polymer chains tends to engulf the amino groups, reducing their accessibility and reactivity.[36,37]

We then applied the assay to measure the coverage density of HS−PEG−NH_2 chains on the surface of Au nanostructures. Figure 4B shows fluorescence spectra taken from the original HS−PEG−NH_2 solutions and the supernatants after incubation with the 50-nm AuNCs. The decrease in fluorescence intensity corresponds to the amount of HS−PEG−NH_2 that had been conjugated to the surface of AuNCs. By comparing the fluorescent intensities with the calibration curves, the average numbers of HS−PEG−NH_2 molecules attached to the surface of one 50-nm AuNC were estimated to be 24700 ± 1200, 12700 ± 3340 and 2100 ± 740 for −S−PEG_{3000}−NH_2, −S−PEG_{5000}−NH_2, and −S−PEG_{20000}−NH_2, respectively. Herein, the surface area of a AuNC is defined as the outer surface area of a AuNC with the inner surface and pores being excluded since the outer surface is more accessible than

the inner surface due to a relatively small pore size for the AuNC (*ca.* 5 nm in diameter for the 50-nm AuNC). Accordingly, the surface area of a 50-nm AuNC was estimated to be 15000 nm^2. As such, the footprint of an individual $-S-PEG-NH_2$ chain on the surface of 50-nm AuNC could be derived as 0.61, 1.18, and 7.14 nm^2, for $-S-PEG_{3000}-NH_2$, $-S-PEG_{5000}-NH_2$ and $-S-PEG_{20000}-NH_2$, respectively. Accordingly, the coverage densities of PEG chains were 1.64, 0.85, and 0.14 per nm^2 for $-S-PEG_{3000}-NH_2$, $-S-PEG_{5000}-NH_2$, and $-S-PEG_{20000}-NH_2$, respectively.

Quantification Using the Ninhydrin-Based Assay. In the ninhydrin-based assay, ninhydrin reacts with the primary amine to generate a chromophore in deep blue or purple color, known as Ruhemann's purple (Figure S6).[25] In a typical reaction, the color was developed over a short period of time depending on the reactivity of the amine group and could reach a maximum intensity in 4 min.[26] Figure 5A shows the calibration curves for $HS-PEG-NH_2$ that correlate the absorbance at 565 nm with the concentration of $HS-PEG-NH_2$. Similar to the fluorescamine-based assay, linear relationships were found up to μM concentrations with the slopes decreasing in the order of $HS-PEG_{3000}-NH_2 > HS\text{-}PEG_{5000}-NH_2 > HS-PEG_{20000}-NH_2$. In general, the detection sensitivity of ninhydrin-based assay was much lower than that of fluorescamine-based assay. For example, $HS-PEG_{5000}-NH_2$ could still be detected at a concentration of 250 nM by the fluorescamine-based assay (Supporting Information, Figure S4A) while it became very difficult to measure using the ninhydrin-based assay at a concentration of 500 nM (Figure S4B). Figure 5B shows the UV–vis spectra taken from the original $HS-PEG-NH_2$ solution and from the supernatants after incubation with 50-nm AuNCs. The drop in absorbance was directly proportional to the number of $HS-PEG-NH_2$ molecules that had been attached to the surface of AuNCs. The average numbers of $-S-PEG-NH_2$ per AuNC were found to be 33170 ± 2750, 20000 ± 2400, and 3200 ± 1770 for $-S-PEG_{3000}-NH_2$, $-S-PEG_{5000}-NH_2$, and $-S-PEG_{20000}-NH_2$, respectively. The coverage densities of PEG chains were 2.21, 1.33, and 0.21 per nm^2 for $-S-PEG_{3000}-NH_2$, $-S-PEG_{5000}-NH_2$, and $-S-PEG_{20000}-NH_2$, respectively.

Both fluorescamine- and ninhydrin-based assays gave the number of unreacted $HS-PEG-NH_2$ molecules in the solution, which could then be converted to the number of $-S-PEG-NH_2$ chains on the surface of AuNCs. As shown in Table 1, the ninhydrin-based assay was found to consistently give a larger number of PEG chains per AuNC as compared to the fluorescamine-based assay. The discrepancy between these two assays could be attributed to a phenomenon known as metal-enhanced fluorescence (MEF).[38,39] Although both assays measured the number of unreacted $HS-PEG-NH_2$ molecules in the supernatant, any small amount of AuNCs left in the supernatant might enhance the fluorescence intensity while causing no change to the absorbance because there was no overlap between the absorption peaks of AuNCs and the dye. As a result, the fluorescamine-based assay tended to produce a smaller difference for the samples before and after PEGylation, thus giving a smaller number of PEG chains on each AuNC in comparison with the ninhydrin-based assay. In general, the ninhydrin-based assay is less sensitive to the sample preparation procedure (*e.g.*, complete sedimentation of all AuNCs or not) and should be more reliable for quantifying the number of $-S-PEG-NH_2$ chains. As a compromise, the ninhydrin-based assay has a much lower detection sensitivity compared to the fluorescamine-based assay. Depending on the physical properties of the sample, one needs to carefully choose a proper quantification method.

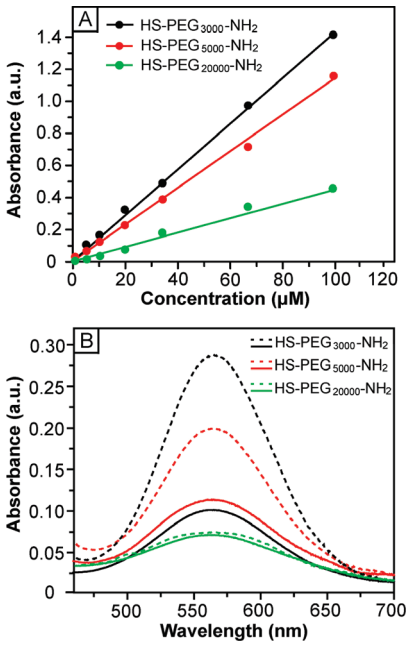

Figure 5. (A) Calibration curves for $HS-PEG-NH_2$ and ninhydrin-based assay, showing a linear relationship between the absorbance at 565 nm and the concentration of $HS-PEG-NH_2$. (B) UV–vis spectra of the chromophore derived from a reaction between ninhydrin and $HS-PEG_{3000}-NH_2$ (black curves), $HS-PEG_{5000}-NH_2$ (red curves), and $HS-PEG_{20000}-NH_2$ (green curves), respectively. The dotted and solid curves correspond to spectra taken from the original solution and from the supernatant after incubation with 50-nm AuNCs for 12 h, respectively.

Quantification Using an Assay Based on FITC-Labeling. In this assay, FITC molecules were added and coupled to the $-NH_2$ groups on $Au-S-PEG-NH_2$ conjugates through a reaction involving isothiocyanate and amino groups. After conjugation, the fluorescence from FITC attached to the surface of Au nanostructures is typically quenched due to a strong interaction between the electrons on the metal surface and the dipole of the dye, a phenomenon known as nanosurface energy transfer (NSET).[40,41] To recover the fluorescence, an

TABLE 1. Characterization of the AuNCs before and after Functionalization with HS−PEG−NH_2.[a]

HS−PEG−NH_2 (Dalton)	hydrodynamic diameter (nm)	zeta potential (mV)	total PEGs per AuNC[b]	total PEGs per AuNC[c]	active PEGs per AuNC[d]	active PEGs per AuNC[e]
no PEG	96.1	−47.9				
3000	108.1	20.3	24700 ± 1200	33170 ± 2750	8860 ± 990	7000 ± 3200
5000	130.1	11.7	12700 ± 3340	20000 ± 2400	4760 ± 870	3800 ± 2100
20000	113.9	−35	2100 ± 740	3200 ± 1770	1010 ± 620	760 ± 400

[a] The edge length of the AuNCs was measured to be 50 nm by TEM. [b] Measured by the fluorescamine-based assay. [c] Measured by the ninhydrin-based assay. [d] Measured by the FITC-labeling assay. [e] Measured by the Cu^{2+}-labeling assay.

aqueous KCN solution was added to completely dissolve the Au nanostructures, releasing the −S−PEG−FITC chains from the metal surface, probably in the form of disulfide. The intensity of fluorescence from the released -S−PEG−FITC is directly proportional to the number of "active" $-NH_2$ groups that could react with FITC. Figure 6 shows fluorescence spectra recorded from the −S−PEG−FITC molecules in three different lengths that had been released from the surface of 50-nm AuNCs. By comparing with a calibration curve (Figure S7), the average numbers of "active" $-NH_2$ groups were found to be 8860 ± 990, 4760 ± 870 and 1010 ± 620 for $-S-PEG_{3000}-NH_2$, $-S-PEG_{5000}-NH_2$, and $-S-PEG_{20000}-NH_2$, respectively. The percentages of "active" $-NH_2$ groups for FITC conjugation *versus* the total $-S-PEG-NH_2$ chains measured using the fluorescamine-based assay were 35.9%, 37.5%, and 48.1% for $-S-PEG_{3000}-NH_2$, $-S-PEG_{5000}-NH_2$, and $-S-PEG_{20000}-NH_2$, respectively.

Quantification Using an Assay Based on Cu^{2+}-Labeling. In this method, the $-NH_2$ groups on the surface of Au−S−PEG−NH_2 conjugates were initially coupled with DOTA−NHS through an amide coupling reaction *via* NHS-activated ester, followed by loading of Cu^{2+} ions.[42−44] The resultant Au−S−PEG−DOTA−Cu^{2+} conjugates were then digested using *aqua regia* for ICP−MS measurement. The numbers of "active" $-NH_2$ groups on each AuNC were then derived from the numbers of loaded Cu^{2+} ions, which were found to be 7000 ± 3200, 3800 ± 2100 and 760 ± 400 for $-S-PEG_{3000}-NH_2$, $-S-PEG_{5000}-NH_2$, and $-S-PEG_{20000}-NH_2$, respectively, per 50-nm AuNC. The percentages of "active" $-NH_2$ groups for DOTA conjugation and Cu^{2+} loading relative to the number of $-S-PEG-NH_2$ chains measured by the fluorescamine-based assay was 28.3%, 29.9%, and 36.2% for $-S-PEG_{3000}-NH_2$, $-S-PEG_{5000}-NH_2$, and $-S-PEG_{20000}-NH_2$, respectively. This trend was similar to what was obtained using an assay based on FITC-labeling. However, the number of active PEG−NH_2 units per 50-nm AuNC measured using the Cu^{2+}-labeling assay was lower than what was obtained using the FITC-labeling method. The discrepancy can be attributed to the difference in conjugation procedure: The FITC-labeling assay involved one-step conjugation while the Cu^{2+}-labeling assay required the use of two steps. In general, the coupling efficiency of a two-step process is always lower than that of a one-step process.

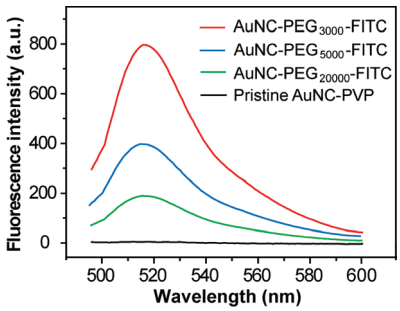

Figure 6. Fluorescence spectra of the solutions containing AuNC−S−PEG−FITC after the AuNCs had been dissolved with a KCN-based etchant: AuNC−S−PEG_{3000}−FITC (10 pM, red curve), AuNC−S−PEG_{5000}−FITC (10 pM, blue curve), AuNC−S−PEG_{20000}−FITC (20 pM, green curve) and the pristine AuNC (20 pM, black curve).

Characterization of the AuNC−S−PEG−NH_2 Conjugates. The hydrodynamic diameter and zeta potential of the AuNCs were expected to change as PVP was replaced by $-S-PEG-NH_2$ (Table 1). We used DLS to measure the hydrodynamic diameters and zeta potentials of the nanoparticles. After PEGylation, the AuNCs showed an increase in hydrodynamic diameter, suggesting that $-S-PEG-NH_2$ chains had been attached to the surface of AuNCs. In comparison with AuNC−S−$PEG_{3000}-NH_2$, the hydrodynamic diameter of AuNC−S−$PEG_{5000}-NH_2$ was increased by 22.6 nm due to the increased molecular weight for PEG. These two PEGs can both self-assemble as a brush-like structure on the surface of AuNC, and thus the hydrodynamic diameter is mainly determined by the PEG chain length.[45] For $-S-PEG_{20000}-NH_2$, however, the polymer chain tended to coil and take a mushroom-like conformation on the surface of AuNC.[31,32] As a result, the hydrodynamic diameter of AuNC−S−$PEG_{20000}-NH_2$ was smaller than that of AuNC−S−$PEG_{5000}-NH_2$. The surface modification by $-S-PEG-NH_2$ was also confirmed by the changes to surface charge before and after conjugation through zeta potential measurements. After PEGylation, the AuNCs showed an increase in zeta potential, which could be ascribed to the presence of positively charged $-NH_2$ groups on the AuNC−S−PEG−NH_2 conjugates at pH ≈ 6.7 (deionized water). The zeta potentials decreased in the order of AuNC−S−$PEG_{3000}-NH_2$ (highly positive) > AuNC−S−$PEG_{5000}-NH_2$

(positive) ≫ AuNC−S−PEG_{20000}−NH_2 (slightly negative) > PVP-capped AuNC (negative). This trend is in agreement with the hydrodynamic diameter measurement and could provide some indirect information about the coverage density of −S−PEG−NH_2 chains on AuNCs, as well as the polymer chain conformation.

Adsorption Kinetics of HS−PEG−NH_2. We also studied the adsorption kinetics of HS−PEG−NH_2 for the functionalization of different types of Au nanostructures. The adsorption of a HS-containing aliphatic molecule onto a Au surface occurs very quickly, typically in few minutes, at room temperature.[20,46] To monitor the adsorption kinetics, the conjugation of Au nanostructures with HS−PEG−NH_2 was performed at 0 °C in an ice bath. The fluorescamine-based assay was chosen to quantify the coverage density of −S−PEG−NH_2 chains at different reaction times (t) due to its high sensitivity. Figure 7 compares the adsorption kinetics for HS−PEG_{5000}−NH_2 and Au nanostructures covered with different capping ligands. For PVP-capped AuNCs, fast kinetics was involved at the initial stage, by which 50% of the −S−PEG−NH_2 chains had been adsorbed onto the surface of AuNCs at $t \approx 10-15$ min. After 20 min, the −S−PEG−NH_2 chains seemed to undergo a reorganization process through desorption and adsorption and finally the coverage density of PEG−NH_2 chains reached a plateau at $t \approx 100$ min. The CTAC-capped AuNPs showed kinetics similar to what was observed for the PVP-capped AuNCs. For citrate-capped AuNPs, at $t \approx 5-10$ min, 50% of −S−PEG−NH_2 chains were found to be adsorbed onto the surface of AuNPs, which was faster than the above two cases. An equilibrium state was reached at $t \approx 60$ min. In the case of CTAB-capped AuNRs, however, much longer periods of time were required to reach both 50% coverage (at $t \approx 20-30$ min) and an equilibrium state (at $t \approx 150$ min).

The Effects of Particle Size and Capping Ligand on PEGylation. We investigated the effect of particle size on the efficiency of PEGylation by employing AuNCs with different edge lengths. For this purpose, 30-, 50- and 60-nm AuNCs (Figure 2A−C) were conjugated with HS−PEG_{5000}−NH_2 using the standard procedure at 4 °C. The average numbers of −S−PEG_{5000}−NH_2 chains per AuNC were found to be 3300 ± 1040, 12700 ± 3340 and 29500 ± 8980, respectively, using the fluorescamine-based assay. The coverage densities of −S−PEG_{5000}−NH_2 chains on the 30-, 50-, and 60-nm AuNCs were calculated as 0.61, 0.85, and 1.36 per nm^2, respectively. As the AuNCs became smaller, the areas of both corners and edges would increase relative to the side faces.[47] Because of the presence of curvature at the corner or edge site, the PEG chains would not be able to interact strongly or pack densely, so it is not unreasonable to expect the coverage density of PEG chains to drop as the particle size was reduced.

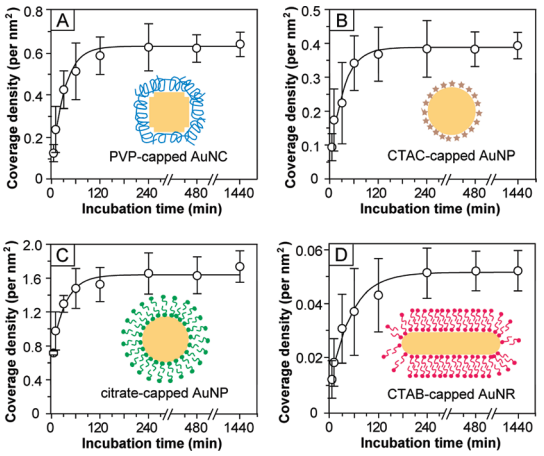

Figure 7. Adsorption kinetics for the PEGylation of various types of Au nanostructures with HS−PEG_{5000}−NH_2 as measured by the fluorescamine-based assay. The error bars represent standard deviation from six replicas for each measurement. The inset depicts the morphology of each type of Au nanostructure and its surface capping layer.

The initial capping ligand on the surface of Au nanostructures is also expected to play an important role in controlling the kinetics of ligand exchange with HS−PEG−NH_2 molecules. To study the effect of capping ligand on PEGylation, Au nanostructures with similar surface areas but capped with different ligands were reacted with HS−PEG_{5000}−NH_2 under the same reaction condition. The Au nanostructures we have examined include PVP-capped AuNCs of 30 nm in edge length, CTAC-capped AuNPs of 40 nm in diameter, citrate-capped AuNPs of 42 nm in diameter, and CTAB-capped AuNRs of 80 nm × 22 nm in dimensions (see Figure 2). They had a similar surface area around 5500 nm^2 (Supporting Information, Figure S8). After incubation with HS−PEG_{5000}−NH_2, the coverage densities of total −S−PEG−NH_2 chains and "active" −NH_2 groups on the surface of these Au NPs were determined using assays based on fluoresceamine and FITC-labeling, respectively. As shown in Table 2, the coverage densities of −S−PEG−NH_2 chains on the Au nanostructures decreased in the order of citrate-capped AuNPs > PVP-capped AuNCs ≈ CTAC-capped AuNPs ≫ CTAB-capped AuNRs. This trend implies that the displacement by −S−PEG−NH_2 chains was strongly dependent on the binding affinity of the original capping ligand to the surface of a Au nanostructure, which decreased in the order of CTAB ≫ CTAC ≈ PVP > citrate. We believe that the presence of a compact bilayer of CTAB on the surface of AuNRs was responsible for the low coverage density of −S−PEG−NH_2 chains on the surface of CTAB-capped AuNRs after ligand exchange.[48−50] The coverage densities of "active" −NH_2 groups on these Au nanostructures were found to follow a similar trend in the order of citrate-capped AuNPs > PVP-capped AuNCs ≈ CTAC-capped AuNPs ≫ CTAB-capped AuNRs. The percentage of

TABLE 2. The Coverage Densities of $-S-PEG-NH_2$ Chains on Various Types of Au Nanostructures[a]

gold nanostructures	coverage density of $PEG-NH_2$ chains[b]	coverage density of active $-NH_2$ groups[c]
PVP-capped AuNCs[d]	0.61	0.19
CTAC-capped AuNPs	0.41	0.22
citrate-capped AuNPs	1.63	1.01
CTAB-capped AuNRs	0.052	0.029

[a] The coverage density is defined as the number of $PEG-NH_2$ chains per nm^2 of Au surface. [b] Measured by the fluorescamine-based assay. [c] Measured by the FITC-labeling assay. [d] The inner surface and pores of the AuNCs were not included.

"active" $-NH_2$ groups *versus* total $-S-PEG-NH_2$ chains on the AuNCs was ~30% as compared to a value of ~50% for all three other types of Au NPs. These results imply a low coupling efficiency between FITC and the amino groups on the AuNCs, which is possibly because some of the $-S-PEG-NH_2$ chains diffused through the pores and thus trapped inside the AuNCs. These $-S-PEG-NH_2$ molecules might be poorly accessible to the dye molecules. On the other hand, as compared to AuNPs with large curvature on the surface, the relatively flat surface of AuNCs could increase the packing density of PEG chains and thus reduce the accessibility and reactivity of terminal amino groups on the PEG chains.

CONCLUSIONS

In summary, we have demonstrated four complementary methods for quantitative analysis of the PEGylation efficiency of Au nanostructures, including the coverage density of $-S-PEG-NH_2$ chains and the "active" $-NH_2$ groups, by using assays based on reactions with fluorescamine or ninhydrin, as well as labeling with a dye or Cu^{2+}. For a model system based on $HS-PEG-NH_2$ with different molecular weights and AuNCs with 50 nm in edge length, we found that: (i) the number of $-S-PEG-NH_2$ chains per AuNC decreased in the order of $-S-PEG_{3000}-NH_2 > -S-PEG_{5000}-NH_2 \gg -S-PEG_{20000}-NH_2$; and (ii) the percentage of "active" $-NH_2$ groups *versus* the number of $-S-PEG-NH_2$ chains decreased in the same order. While the fluorescamine-based assay was much more sensitive than the ninhydrin-based assay, the latter was less sensitive to the experimental details and thus most reliable among all four methods. The Cu^{2+}-labeling assay was less efficient than the assay based on FITC-labeling because of the involvement of a two-step procedure. The initial capping ligand on the Au nanostructures played a key role in determining both the efficiency and kinetics of the ligand exchange process. This study provides a set of useful guidelines for PEGylation of Au nanostructures, as well as for surface modification with other compounds or polymers, in an effort to improve the *in vivo* delivery of nanomaterials.

METHODS

Chemicals and Materials. Fluorescamine was purchased from Invitrogen (Carlsbad, CA). $HS-PEG_{5000}-NH_2$ (MW ≈ 5000) and $HS-PEG_{20000}-NH_2$ (MW ≈ 20000) were purchased from Laysan Bio (Arab, AL), $HS-PEG_{3000}-NH_2$ (MW ≈ 3000) was obtained from Rapp Polymere GmbH (Tübingen, Germany). 1,4,7,10-Tetraazacyclododecane-1,4,7,10-tetreaacetic acid mono(*N*-hydroxysuccinimide ester) (DOTA–NHS, ≥90%) was obtained from Macrocyclics (Dallas, TX). The Kaiser test kit was obtained from Fluka (Buchs, Switzerland). Fluorescein isothiocyanate (FITC, ~98%), Chelex 100 resin (50–100 mesh), copper(II) chloride ($CuCl_2$, ~99.9%), gold(III) chloride trihydrate ($HAuCl_4 \cdot 3H_2O$, ≥99.0%), sodium borohydride ($NaBH_4$, 99%), L-ascorbic acid (>99%), silver nitrate ($AgNO_3$, >99%), poly(vinyl pyrrolidone) (PVP, MW ≈ 55000), cetyltrimethylammonium bromide (CTAB, ≥99%), cetyltrimethylammonium chloride (CTAC, ≥98%), and 1,10-phenanthroline ethylenediaminetetraacetic acid (EDTA, ≥99%) were all obtained from Sigma-Aldrich (St. Louis, MO). All the chemical reagents were used as received. Water with a resistivity of 18 MΩ·cm was prepared using a E-Pure filtration system from Barnstead International (Dubuque, IA). The water and buffer solutions used for Cu^{2+} labeling were treated with Chelex 100 overnight prior to use.

Synthesis of Au Nanostructures. The 30-, 50-, and 60-nm AuNCs covered by PVP were synthesized using a published procedure.[51] The 40-nm AuNPs capped by CTAC were prepared using a recently reported, two-step procedure.[52] Synthesis of the 42-nm AuNPs capped by citrate ions was conducted using the citrate reduction method.[53] The AuNRs capped by CTAB were prepared using the procedure reported by El-Sayed and co-workers.[54]

PEGylation of Au Nanostructures with $HS-PEG-NH_2$. In a typical process, 1.2 mL of a 0.25 mM aqueous $HS-PEG-NH_2$ solution was added to 3 mL of an aqueous suspension of Au nanostructures (1.7 nM), followed by addition of 1.8 mL of H_2O to a total volume of 6 mL. The final concentration of Au nanostructures and $HS-PEG-NH_2$ were 0.85 nM and 50 μM, respectively. The reaction mixture was vortexed immediately and then incubated at 4 °C overnight, followed by centrifuging at 14000 rpm for 5 min. The supernatant was carefully collected, and centrifuged two more times to remove the remaining Au nanostructures. The resultant supernatant solution was subjected to the fluorescamine- and ninhydrin-based assays to determine the number of unreacted $HS-PEG-NH_2$ molecules. The $HS-PEG-NH_2$-functionalized Au nanostructures were washed three more times and then used for conjugation with FITC or DOTA–NHS for corresponding measurements.

Quantification of $-S-PEG-NH_2$ Chains on Au Nanostructures Using Fluorescamine-Based Assay. Prior to analysis, a calibration curve was obtained from a series of $HS-PEG-NH_2$ solutions with known concentrations. Briefly, to each 3 mL of $HS-PEG-NH_2$ standard phosphate buffered (PB, pH = 10) solution, 0.25 mL of 2 μM fluorescamine solution in acetone was added. After 15 min, fluorescence spectra ($\lambda_{ex} \approx 390$ nm, $\lambda_{em} \approx 480$ nm) were recorded. The fluorescent intensities at 480 nm for each solution were plotted as a function of the concentration of $HS-PEG-NH_2$ to generate a calibration curve. For sample measurements, 100 μL of the supernatant solution was diluted into 3 mL with the PB buffer and treated using a procedure similar to what was used for the calibration curve. By comparing the fluorescence intensities with the calibration curve and multiplying the dilution factors, we obtained the concentrations of $HS-PEG-NH_2$ in the supernatant solutions. The number of $HS-PEG-NH_2$ on the Au nanostructures was obtained by subtracting the number of $HS-PEG-NH_2$ in the supernatant from the total number of $HS-PEG-NH_2$ added into the suspension of Au nanostructures. This number was then converted to the coverage density by taking into account the total number of Au nanostructures and their total surface area. Each data point represents an average of three replicas.

Quantification of $-S-PEG-NH_2$ Chains on Au Nanostructures Using Ninhydrin-Based Assay. All reagents used for the assay were prepared according to the literature.[55−57] Typically, 6% ninhydrin ethanol solution was prepared by dissolving 2.5 g of ninhydrin in 50 mL of anhydrous ethanol. The KCN pyridine solution and 80% phenol solution in ethanol from the Kaiser test kit were combined at a 1:1 volume ratio to give a KCN/phenol solution. Prior to assay, a calibration curve was obtained from a series of $HS-PEG-NH_2$ standard solutions with known concentrations. Briefly, to each 250 μL of $HS-PEG-NH_2$ standard solutions, 100 μL of 6% ninhydrin ethanol solution and 200 μL of KCN/phenol solution were added, followed by heating at 100 °C for 4 min. After being cooled down in an ice bath, 200 μL of 60 wt % ethanol in water was added. UV−vis spectra were then recorded. The calibration curve was generated by plotting the absorbance at 565 nm as a function of the $HS-PEG-NH_2$ concentration. Samples of 250 μL (the supernatant solution) were treated using the same procedure as that used for standard solutions. The number of overall $HS-PEG-NH_2$ on the Au nanoparticle was calculated using the same method as that of the fluorescamine-based assay. Each data point represents an average of three replicas.

Quantification of Active $-NH_2$ Groups on Au Nanostructures by Dye-Labeling Assay. To 500 μL of $Au-S-PEG-NH_2$ (with a known concentration), 2 μL of 50 mM FITC in dimethyl sulfoxide (DMSO) was added. The reaction mixture was incubated at room temperature for 15 min, followed by five times washing with water. The pellet was redispersed in 500 μL of water. To the pellet suspension, 2.5 mL of 40 mM KCN aqueous solution and 2.0 mL of water was added to dissolve the Au nanoparticles at room temperature for 30 min. After that, fluorescent spectra ($\lambda_{ex} \approx 488$ nm, $\lambda_{em} \approx 520$ nm) were taken from the sample. The concentration of FITC in each sample was calculated by comparing with the calibration curve obtained for free FITC aqueous solution. The number of active $-NH_2$ groups per Au nanoparticle was calculated from the numbers of FITCs and Au nanoparticles. Each data point represents an average of three replicas.

Quantification of Active $-NH_2$ Groups on Au Nanostructures by Cu^{2+}-Labeling Assay. A 500 μL portion of 0.4 nM $Au-S-PEG-NH_2$ was washed three times with chelexed water and resuspended in 500 μL of chelexed water. Then, 500 μL of 1 mM DOTA−NHS in 0.1 M PB buffer (pH = 7.4) was added. The reaction mixture was incubated at room temperature for 1 h, followed by washing five times with chelexed water. After the final round of centrifugation, 1 mL of 0.1 M NaOAc buffer (pH = 5.5) was added to resuspend the pellet, followed by the addition of 10 μL of $CuCl_2$ aqueous solution (50 mM). After incubation at 37 °C for 1 h, 500 μL of 1 mM EDTA aqueous solution was added to chelate the unbound Cu^{2+} ions for 15 min. The mixture was washed five times with chelexed water to remove the EDTA−Cu^{2+}, resulting in Au−PEG−DOTA−Cu^{2+}. For Cu^{2+} analysis, 5 μL of the sample solution was dissolved in 0.5 mL of concentrated *aqua regia* and further diluted to 30 mL using 1% HNO_3 aqueous solution prior to ICP−MS measurement. The number of active $-NH_2$ groups per Au nanoparticle could be estimated from the ratio of Cu^{2+} ions to Au nanoparticles from ICP−MS analysis. Each data point represents an average of three replicas.

Instrumentation. TEM images of the Au nanostructures were obtained with a Technai G2 Spirit microscope operated at 120 kV (FEI). Fluorescence spectra were recorded using a Cary Eclipse fluorescence spectrophotometer (Varian). UV−vis spectra were taken with a Cary 50 UV−vis spectrophotometer (Varian). The hydrodynamic diameter of the Au nanostructures was measured in deionized water (pH ≈ 6.7) using dynamic light scattering (Malvern, NanoZS) which was equipped with a zeta-potential analyzer. The concentrations of Au, Ag, and Cu elements were determined using ICP−MS (Perkin-Elmer, Elan DRC II). The concentration of Au element was then converted to the concentration of Au nanostructures once the particle size and morphology had been determined by TEM.

Acknowledgment. This work was supported in part by a grant from NCI (1R01 CA138527), an NIH Director's Pioneer Award (DP1 OD000798), and startup funds from Washington University in St. Louis. As a jointly supervised Ph.D. student from Xiamen University, X.X. was also partially supported by a fellowship from the China Scholarship Council.

Supporting Information Available: UV−vis spectra of the 50-nm AuNCs before and after functionalization with $HS-PEG_{3000}-NH_2$ or $HS-PEG_{3000}-COOH$ at 4 and 22 °C; scheme of the reaction involving a primary amine and fluorescamine (or ninhydrin); typical excitation and emission spectra of the chromophore derived from fluorescamine and $HS-PEG-NH_2$; fluorescence and UV−vis spectra of $HS-PEG_{5000}-NH_2$ standard solutions; calibration curve obtained for $HS-PEG_{5000}-NH_2$ at pH = 6.5 using the fluorescamine-based assay; calibration curve for free FITC; calculations of surface areas for different types of Au nanostructures; and a table of characterization of AuNCs with different surface coatings under different temperatures. This material is available free of charge *via* the Internet at http://pubs.acs.org.

REFERENCES AND NOTES

1. Cho, E. C.; Glaus, C.; Chen, J.; Welch, M. J.; Xia, Y. Inorganic Nanoparticle-Based Contrast Agents for Molecular Imaging. *Trends Mol. Med.* **2010**, *16*, 561–573.
2. Peer, D.; Karp, J. M.; Hong, S.; Farokhzad, O. C.; Margalit, R.; Langer, R. Nanocarriers as an Emerging Platform for Cancer Therapy. *Nat. Nanotechnol.* **2007**, *2*, 751–760.
3. Rosi, N. L.; Mirkin, C. A. Nanoparticles in Biodiagnostics. *Chem. Rev.* **2005**, *105*, 1547–1562.
4. Lal, S.; Clare, S. E.; Halas, N. J. Nanoshell-Enabled Photothermal Cancer Therapy: Impending Clinical Impact. *Acc. Chem. Res.* **2008**, *41*, 1842–1851.
5. Jain, P. K.; Huang, X.; El-Sayed, I. H.; El-Sayed, M. A. Noble Metals on the Nanoscale: Optical and Photothermal Properties and Some Applications in Imaging, Sensing, Biology, and Medicine. *Acc. Chem. Res.* **2008**, *41*, 1578–1586.
6. Xia, Y.; Li, W.; Cobley, C. M.; Chen, J.; Xia, X.; Zhang, Q.; Yang, M.; Cho, E. C.; Brown, P. K. Gold Nanocages: From Synthesis to Theranostic Applications. *Acc. Chem. Res.* **2011**, *44*, 914–924.
7. Murphy, C. J.; Gole, A. M.; Stone, J. W.; Sisco, P. N.; Alkilany, A. M.; Goldsmith, E. C.; Baxter, S. C. Gold Nanoparticles in Biology: Beyond Toxicity to Cellular Imaging. *Acc. Chem. Res.* **2008**, *41*, 1721–1730.
8. Tong, L.; Zhao, Y.; Huff, T. B.; Hansen, M. N.; Wei, A.; Cheng, J.-X. Gold Nanorods Mediate Tumor Cell Death by Compromising Membrane Integrity. *Adv. Mater.* **2007**, *19*, 3136–3141.
9. Duncan, B.; Kim, C.; Rotello, V. M. Gold Nanoparticle Platforms as Drug and Biomacromolecule Delivery Systems. *J. Controlled Release* **2010**, *148*, 122–127.
10. Bardhan, R.; Lal, S.; Joshi, A.; Halas, N. J. Theranostic Nanoshells: From Probe Design to Imaging and Treatment of Cancer. *Acc. Chem. Res.* **2011**, *44*, 936–946.
11. Harris, J. M., Ed. *Poly(ethylene glycol) Chemistry: Biotechnical and Biomedical Applications*; Plenum Press: New York, 1992.
12. Karakoti, A. S.; Das, S.; Thevuthasan, S.; Seal, S. PEGylated Inorganic Nanoparticles. *Angew. Chem., Int. Ed.* **2011**, *50*, 1980–1994.
13. Neoh, K. G.; Kang, E. T. Functionalization of Inorganic Nanoparticles with Polymers for Stealth Biomedical Applications. *Pol. Chem.* **2011**, *2*, 747–759.
14. Knop, K.; Hoogenboom, R.; Fischer, D.; Schubert, U. S. Poly(ethylene glycol) in Drug Delivery: Pros and Cons as Well as Potential Alternatives. *Angew. Chem., Int. Ed.* **2010**, *49*, 6288–6308.
15. Unsworth, L. D.; Sheardown, H.; Brash, J. L. End-Thiolated Poly(ethylene glycol) to Gold: Effect of Surface Chain Density. *Langmuir* **2005**, *21*, 1036–1041.

16. Perrault, S. D.; Walkey, C.; Jennings, T.; Fischer, H. C.; Chan, W. C. W. Mediating Tumor Targeting Efficiency of Nanoparticles through Design. *Nano Lett.* **2009**, *9*, 1909–1915.
17. Pale-Grosdemange, C.; Simon, E. S.; Prime, K. L.; Whitesides, G. M. Formation of Self-Assembled Monolayers by Chemisorption of Derivatives of Oligo(ethylene glycol) of Structure $HS(CH_2)_{11}(OCH_2CH_2)mOH$ on Gold. *J. Am. Chem. Soc.* **1991**, *113*, 12–20.
18. Latham, A. H.; Williams, M. E. Versatile Routes toward Functional, Water-Soluble Nanoparticles *via* Trifluoroethylester–PEG–Thiol Ligands. *Langmuir* **2006**, *22*, 4319–4326.
19. Hong, R.; Fischer, N. O.; Emrick, T.; Rotello, V. M. Surface PEGylation and Ligand Exchange Chemistry of FePt Nanoparticles for Biological Applications. *Chem. Mater.* **2005**, *17*, 4617–4621.
20. Love, J. C.; Estroff, L. A.; Kriebel, J. K.; Nuzzo, R. G.; Whitesides, G. M. Self-Assembled Monolayers of Thiolates on Metals as a Form of Nanotechnology. *Chem. Rev.* **2005**, *105*, 1103–1170.
21. Wuelfing, W. P.; Gross, S. M.; Miles, D. T.; Murray, R. W. Nanometer Gold Clusters Protected by Surface-Bound Monolayers of Thiolated Poly(ethylene glycol) Polymer Electrolyte. *J. Am. Chem. Soc.* **1998**, *120*, 12696–12697.
22. Stark, G. R. Reactions of Cyanate with Functional Groups of Proteins. III. Reactions with Amino and Carboxyl Groups. *Biochemistry* **1965**, *4*, 1030–1036.
23. Bender, M. L. Mechanisms of Catalysis of Nucleophilic Reactions of Carboxylic Acid Derivatives. *Chem. Rev.* **1960**, *60*, 53–113.
24. Udenfriend, S.; Stein, S.; Böhlen, P.; Dairman, W.; Leimgruber, W.; Weigele, M. Fluorescamine: A Reagent for Assay of Amino Acids, Peptides, Proteins, and Primary Amines in the Picomole Range. *Science* **1972**, *178*, 871–872.
25. Kaiser, E.; Colescott, R. L.; Bossinger, C. D.; Cook, P. I. Color Test for Detection of Free Terminal Amino Groups in the Solid-Phase Synthesis of Peptides. *Anal. Biochem.* **1970**, *34*, 595–598.
26. Sarin, V. K.; Kent, S. B. H.; Tam, J. P.; Merrifield, R. B. Quantitative Monitoring of Solid-Phase Peptide Synthesis by the Ninhydrin Reaction. *Anal. Biochem.* **1981**, *117*, 147–157.
27. Ramachandran, G. K.; Hopson, T. J.; Rawlett, A. M.; Nagahara, L. A.; Primak, A.; Lindsay, S. M. A Bond-Fluctuation Mechanism for Stochastic Switching in Wired Molecules. *Science* **2003**, *300*, 1413–1416.
28. Kamenetska, M.; Koentopp, M.; Whalley, A. C.; Park, Y. S.; Steigerwald, M. L.; Nuckolls, C.; Hybertsen, M. S.; Venkataraman, L. Formation and Evolution of Single-Molecule Junctions. *Phys. Rev. Lett.* **2009**, *102*, 126803.
29. Frei, M.; Aradhya, S. V.; Koentopp, M.; Hybertsen, M. S.; Venkataraman, L. Mechanics and Chemistry: Single Molecule Bond Rupture Forces Correlate with Molecular Backbone Structure. *Nano Lett.* **2011**, *11*, 1518–1523.
30. Aina, V.; Marchis, T.; Laurenti, E.; Diana, E.; Lusvardi, G.; Malavasi, G.; Menabue, L.; Cerrato, G.; Morterra, C. Functionalization of Sol Gel Bioactive Glasses Carrying Au Nanoparticles: Selective Au Affinity for Amino and Thiol Ligand Groups. *Langmuir* **2010**, *26*, 18600–18605.
31. Yang, Z. H.; Galloway, J. A.; Yu, H. Protein Interactions with Poly(ethylene glycol) Self-Assembled Monolayers on Glass Substrates: Diffusion and Adsorption. *Langmuir* **1999**, *15*, 8405–8411.
32. Tsukanova, V.; Salesse, C. On the Nature of Conformational Transition in Poly(ethylene glycol) Chains Grafted onto Phospholipid Monolayers. *J. Phys. Chem. B* **2004**, *108*, 10754–10764.
33. Wanwimolruk, S.; Birkett, D. J.; Brooks, P. M. Structural Requirements for Drug Binding to Site II on Human Serum Albumin. *Mol. Pharmacol.* **1983**, *24*, 458–463.
34. Matsuura, H.; Fukuhara, K. Conformational Analysis of Poly(oxyethylene) Chain in Aqueous Solution as a Hydrophilic Moiety of Nonionic Surfactants. *J. Mol. Struct.* **1985**, *126*, 251–260.
35. Yoshihara, T; Tadokoro, H; Murahashi, S. Normal Vibrations of the Polymer Molecules of Helical Conformations. IV. Polyethylene Oxide and Polyethylene-d_4 Oxide. *J. Chem. Phys.* **1964**, *41*, 2902–2911.
36. Ahmad, B.; Ansari, M. A.; Sen, P.; Khan, R. H. Low *versus* High Molecular Weight Poly(ethylene glycol)-Induced States of Stem Bromelain at Low pH: Stabilization of Molten Globule and Unfolded States. *Biopolymers* **2006**, *81*, 350–359.
37. Chaput, S. B.; Carrot, C. Interactions of Active Carbon with Low- and High-Molecular Weight Polyethylene Glycol and Polyethylene Oxide. *J. App. Polym. Sci.* **2006**, *100*, 3490–3497.
38. Sokolov, K.; Chumanov, G.; Cotton, T. M. Enhancement of Molecular Fluorescence near the Surface of Colloidal Metal Films. *Anal. Chem.* **1998**, *70*, 3898–3905.
39. Geddes, C. D.; Lakowicz, J. R. Editorial: Metal-Enhanced Fluorescence. *J. Fluoresc.* **2002**, *12*, 121–129.
40. Xia, X.; Yang, M.; Oetjen, L. K.; Zhang, Y.; Li, Q.; Chen, J.; Xia, Y. An Enzyme-Sensitive Probe for Photoacoustic Imaging and Fluorescence Detection of Protease Activity. *Nanoscale* **2011**, *3*, 950–953.
41. Yun, C. S.; Javier, A.; Jennings, T.; Fisher, M.; Hira, S.; Peterson, S.; Hopkins, B.; Reich, N. O.; Strouse, G. F. Nanometal Surface Energy Transfer in Optical Rulers, Breaking the FRET Barrier. *J. Am. Chem. Soc.* **2005**, *127*, 3115–3119.
42. Li, W. P.; Meyer, L. A.; Capretto, D. A.; Sherman, C. D; Anderson, C. J. Receptor Binding, Biodistribution, and Metabolism Studies of ^{64}Cu-DOTA-Cetuximab, a PET Imaging Agent for Epidermal Growth-Factor Receptor-Positive Tumors. *Cancer Biother. Radiopharm.* **2008**, *23*, 158–171.
43. Eiblmaier, M.; Meyer, L. A.; Watson, M. A.; Fracasso, P. M.; Pike, L. J.; Anderson, C. J. Correlating EGFR Expression with Receptor-Binding Properties and Internalization of ^{64}Cu-DOTA-Cetuximab in 5 Cervical Cancer Cell Lines. *J. Nucl. Med.* **2008**, *49*, 1472–1479.
44. Jarrett, B. R.; Gustafsson, B.; Kukis, D. L.; Louie, A. Y. Synthesis of ^{64}Cu-labeled Magnetic Nanoparticles for Multimodal Imaging. *Bioconjug. Chem.* **2008**, *19*, 1496–1504.
45. Levin, C. S.; Bishnoi, S. W.; Grady, N. K.; Halas, N. J. Determining the Conformation of Thiolated Poly(ethylene glycol) on Au Nanoshells by Surface-Enhanced Raman Scattering Spectroscopic Assay. *Anal. Chem.* **2006**, *78*, 3277–3281.
46. Weisbecker, C. S.; Merritt, M. V.; Whitesides, G. M. Molecular Self-Assembly of Aliphatic Thiols on Gold Colloids. *Langmuir* **1996**, *12*, 3763–3772.
47. Hostetler, M. J.; Templeton, A. C.; Murray, R. W. Dynamics of Place-Exchange Reactions on Monolayer-Protected Gold Cluster Molecules. *Langmuir* **1999**, *15*, 3782–3789.
48. Nikoobakht, B.; El-Sayed, M. A. Evidence for Bilayer Assembly of Cationic Surfactants on the Surface of Gold Nanorods. *Langmuir* **2001**, *17*, 6368–6374.
49. Gole, A.; Murphy, C. J. Polyelectrolyte-Coated Gold Nanorods: Synthesis, Characterization and Immobilization. *Chem. Mater.* **2005**, *17*, 1325–1330.
50. Yu, C. X.; Varghese, L.; Irudayaraj, J. Surface Modification of Cetyltrimethylammonium Bromide-Capped Gold Nanorods to Make Molecular Probe. *Langmuir* **2007**, *23*, 9114–9119.
51. Skrabalak, S. E; Au, L.; Li, X.; Xia, Y. Facile Synthesis of Ag Nanocubes and Au Nanocages. *Nat. Protoc.* **2007**, *2*, 2182–2190.
52. Ma, Y.; Li, W.; Cho, E. C.; Li, Z.; Yu, T.; Zeng, J.; Xie, Z.; Xia, Y. Au@Ag Core–Shell Nanocubes with Finely Tuned and Well-Controlled Sizes, Shell Thicknesses, and Optical Properties. *ACS Nano* **2010**, *4*, 6725–6734.
53. Frens, G. Controlled Nucleation for the Regulation of the Particle Size in Monodisperse Gold Suspensions. *Nature* **1973**, *241*, 20–22.
54. Nikoobakht, B.; El-Sayed, M. A. Preparation and Growth Mechanism of Gold Nanorods (NRs) Using Seed-Mediated Growth Method. *Chem. Mater.* **2003**, *15*, 1957–1962.

55. Curotto, E.; Aros, F. Quantitative Determination of Chitosan and the Percentage of Free Amino Groups. *Anal. Biochem.* **1993**, *211*, 240–241.
56. Moore, S. J. Amino Acid Analysis: Aqueous Dimethyl Sulfoxide Solvent for the Ninhydrin Reaction. *J. Biol. Chem.* **1968**, *243*, 6281–6283.
57. Sheng, S. J.; Kraft, J. J.; Schuster, S. M. A Specific Quantitative Colorimetric Assay for L-Asparagine. *Anal. Biochem.* **1993**, *221*, 242–249.